Oblique collisions and catching-up phenomena of vortex dipoles in a uniform Bose–Einstein condensate

Guoquan Yang[1], Suying Zhang[1] and Wei Han[2]

[1] Institute of Theoretical Physics, State Key Laboratory of Quantum Optics and Quantum Optics Devices, Shanxi University, Taiyuan, Shanxi 030006, People's Republic of China
[2] Key Laboratory of Time and Frequency Primary Standards, National Time Service Center, Chinese Academy of Sciences, Xi'an 710600, People's Republic of China

E-mail: zhangsy@sxu.edu.cn

Abstract
We investigate the collisional dynamics of two vortex dipoles in a uniform two-dimensional Bose–Einstein condensate. It is found that the dynamics are deeply related to the moving directions and sizes of the initial vortex dipoles. For the oblique collisions of two vortex dipoles with the same size, we find that the vortices in the two initial vortex dipoles recombine into two new vortex dipoles which scatter in the opposite directions. For the catching-up processes of two vortex dipoles with different size, we find that the faster vortex dipole speeds up and passes through the slower vortex dipole. If the size of the vortex dipoles are small, we also observe vortex annihilation and vortex resurrection. The corresponding parameter ranges of different collisional dynamics are discussed.

Keywords: Bose–Einstein condensate, vortex dipole, collision of two vortex dipoles

(Some figures may appear in colour only in the online journal)

1. Introduction

Vortices are persistent circulating flow patterns, which have been observed in most branches of physics such as classical hydrodynamics [1], optical physics [2], superfluids [3] and superconductors [4], as well as cold atomic physics [5–21]. Vortices with opposite circulation move parallel to each other forming a so-called vortex dipole (VD) [22–24]. Although a single vortex carries angular momentum, VDs can be considered as basic topological structures that carry linear momentum in stratified or two-dimentional fluids [25]. VDs are widespread in classical fluid flows, involving ocean currents [26] and soap films [27], exciton-polariton condensate in a semiconductor cavity [28, 29], superfluid helium [30] and ultracold atomic gases. The creation and annihilation of VDs are at the heart of chaotic flows [25] and superfluid phenomena. A quantitative study on the dynamics of VDs will contribute to a broader and deeper understanding of non-equilibrium physics, such as quantum turbulence [30–35],

Berezinskii–Kosterlitz–Thouless transition [36–38], and phase transition dynamics [39–42].

Dynamics of VDs has been recently observed in highly oblate BECs [22]. While in a uniform superfluid the VD propagates with a constant velocity, in an inhomogeneous system it has complicated trajectory [22, 43–45] or even remains stationary [16, 43]. The vortex–antivortex annihilation has also been discussed in [46–51]. Many important works have been performed on the collisional dynamics of VDs in BECs [20, 52, 53]. In [54], Smirnov and his collaborators studied the scattering of VD by a single vortex in a uniform BEC. The results show that the VD was scattered over large angles, in agreement with earlier calculations [55]. In [56], Griffin *et al* studied VD scattering by a fixed impurity potential (whose depth and size is similar to the depth and size of a quantum vortex but without circulation) in a BEC, and compared it with the scattering induced by a target in the form of vortex. In [20], the head-on collision of two VDs in a harmonic trap was studied, and the vortex recombination and
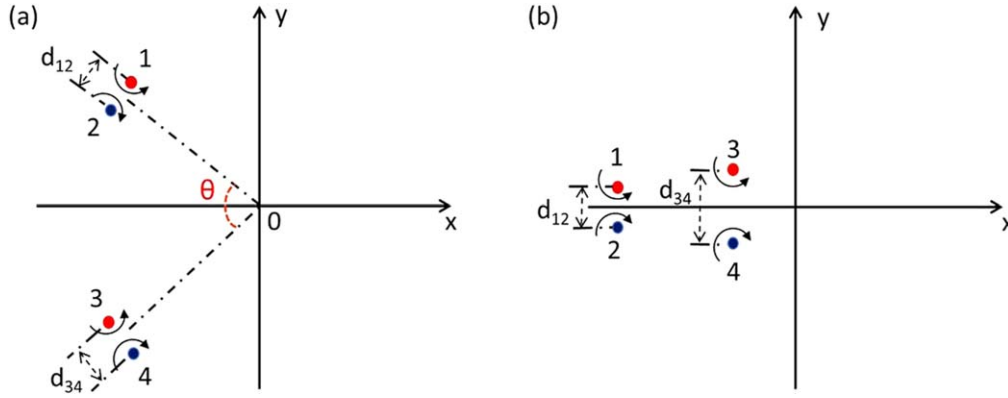
Figure 1. Schematic representation of the interaction of two VDs for the case of (a) oblique collisions and (b) catching-up processes, respectively. Initially, the vortices 1, 3 (red) and the antivortices 2, 4 (blue) are separated by the distances d_{12} and d_{34}. Here θ represents the angle between the moving directions of the two initial VDs.

annihilation were observed by changing the radial position of the initial VDs.

In our previous work [57], we analyzed in detail the parallel collisions of two VDs by varying the parameters, and we identified three general modes, involving the vortex recombination mode, the encircling mode and the flyby mode. However, as far as we know, the effects of the angle θ between the moving directions of two initial VDs on the collisional dynamics have not been studied yet. In this paper, we focus on the dynamics of oblique collisions and catching-up processes of two VDs. Some interesting phenomena, such as vortex recombination, vortex annihilation and vortex resurrection, are predicted. The changes of the velocity and size of the VDs in the collision processes are discussed. We also show the parameter ranges for different collisional dynamics of the VDs.

The rest of the paper is organized as follows. In section 2, we provide the model and numerical method. In section 3, we investigate the dynamics of oblique collision and catching-up process of two VDs. In section 4, we further discuss the reliability of the numerical simulations. Finally, we summarize and give concluding remarks in section 5.

2. The theoretical model and numerical method

In superfluids, a VD propagates with velocity $v_{\mathrm{VD}} \simeq \hbar/(md)$, where m is the atomic mass and d is the separation between the vortex and antivortex [52]. The energy E_{VD} of a VD is calculated by $E_{\mathrm{VD}} \sim \frac{2\pi n_0 \hbar^2}{m} \ln \frac{d}{a_0}$, where n_0 is the atomic density distribution [52]. In a uniform BEC, d is constant in time. In a non-uniform BEC, a VD traveling towards a higher density region will reduce its separation due to energy conservation [50]. So the collisional dynamics of VDs are totally different for uniform and non-uniform BECs. For simplicity, we choose the uniform flat potential to investigate the oblique collisions and catching-up processes of two VDs.

In the weak interaction limit, the quantum dynamics of a BEC is determined by the Gross–Pitaevskii (GP) equation. We restrict the problem to the two-dimensional plane and

consider a uniform cylindrical trap at zero temperature. We model the cylindrical well with $V(\mathbf{r}) = \frac{1}{2}(|\mathbf{r}|/r_0)^\alpha$, where r_0 is the effective radius of the system and α is a parameter which defines the steepness of the trap walls [50]. In the limit of infinite steepness ($\alpha \to \infty$) it approaches a cylindrically symmetric well with radius r_0. There are a variety of techniques for experimentally producing such steep-walled trapping potentials [58, 59]. In this paper, we set $\alpha = 100$ and $r_0 = 20a_0$ to ensure that the condensate is completely confined in the well. Here a_0 is a scaling length parameter relevant to the size of the well. The corresponding characteristic frequency is $\omega_c = \hbar/ma_0^2$. After rescaling the parameters by making the substitution $t \to \omega_c t$, $\mathbf{r} \to \mathbf{r}/a_0$, and $\psi \to \psi/a_0^{3/2}$ [60–63], we can obtain the reduced dimensionless GP equation

$$i\frac{\partial \psi}{\partial t} = -\frac{1}{2}\nabla^2 \psi + V(\mathbf{r})\psi + c\,|\psi|^2\psi, \tag{1}$$

where the interaction strength, $c = 4\pi N a_s/a_0$, is written in terms of the s-wave scattering length a_s, and the total atomic number N. Following a previous work [64], we set $c = 10\,399$. In order to obtain two initial VDs (1, 2 and 3, 4 in figures 1(a) and (b)), we first get the ground state of the system using the imaginary-time method. Then we imprint two VDs in the condensate by multiplying the ground state wave function by a phase factor $\Pi_k^4 \exp(i\theta_k)$, where $\theta_k(x, y) = s_k \arctan[(y - y_k)/(x - x_k)]$. Here, (x_k, y_k) defines the position of the kth vortex, and the sign s_k defending the direction of circulation. After the vortex imprinting, the wave function is evolved further in imaginary time for $0.05\omega_c^{-1}$ to establish the structure of vortex cores. Experimentally, vortices can be seeded into the system by employing the phase imprinting techniques [65–67]. The initial positions of the two VDs are shown in figure 1. The red solid circles represent the vortices, and the blue solid circles represent the antivortices. The sizes of the two VDs are d_{12} and d_{34}, respectively. In figure 1(a), θ represents the angle between the moving directions of the two initial VDs. The initial coordinates (x_k, y_k) of the kth vortex vary from case to case, as we change the collision angle θ. Figure 1(b) is the schematic
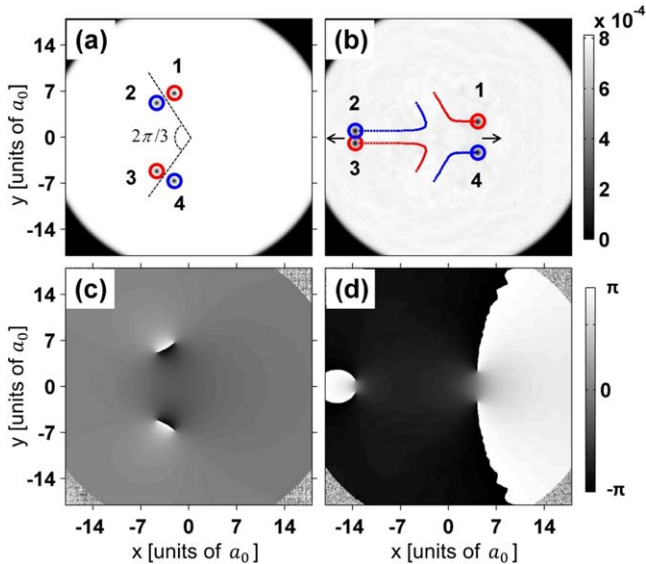
Figure 2. Vortex recombination in the oblique collision dynamics. The positions of the vortices and antivortices are labeled by red and blue circles, respectively. (a) The initial coordinates of the vortices are chosen as $(x_1, y_1) = (-2.12a_0, 6.67a_0)$ (red circle), $(x_2, y_2) = (-4.72a_0, 5.17a_0)$ (blue circle), $(x_3, y_3) = (-4.72a_0, -5.17a_0)$ (red circle) and $(x_4, y_4) = (-2.12a_0, -6.67a_0)$ (blue circle). Then we have $d_{12} = d_{34} = 3a_0$ and $\theta = 2\pi/3$. (b) The trajectories of the vortices (red lines) and antivortices (blue lines) at a time interval of $\Delta t = 40\omega_c^{-1}$. The arrows indicate the directions of the VD propagation after the vortex recombination. The corresponding phase distributions for $t = 0$ and $t = 40\omega_c^{-1}$ are shown in (c) and (d).

Figure 3. The sizes of the VDs as a function of the collision angle θ after the vortex recombination. The size of the initial VDs (1, 2 and 3, 4) are fixed at $d_{1,2} = d_{3,4} = 3a_0$. The sizes of the two new VDs (1, 4 and 2, 3) are represented by black squares (d'_{14}) and green triangles (d'_{23}), respectively.

diagram of the catching-up phenomenon of two VDs, i.e. the case of $\theta = 0$.

We numerically solve equation (1) using the time-splitting Fourier pseudospectral method [68]. The simulations are carried out in a region $(x, y) \in [-25a_0, 25a_0] \times [-25a_0, 25a_0]$ with a refined grid of 768×768 nodes, which is sufficient to achieve grid independence. The time step is set by $\Delta t = 0.001$. The trajectories of the vortices can plotted by searching for their phase signatures [69].

3. Numerical results

3.1. Oblique collision dynamics of two vortex dipoles

We first study the oblique collision of two VDs with the same size $d_{12} = d_{34} = 3a_0$, which are initially located symmetrically on the x-axis with the angle $\theta = 2\pi/3$ between their moving directions, as shown in figure 2(a). When $t = 0$, the four vortices of the two VDs are placed at $(x_1, y_1) = (-2.12a_0, 6.67a_0)$ (red circle), $(x_2, y_2) = (-4.72a_0, 5.17a_0)$ (blue circle), $(x_3, y_3) = (-4.72a_0, -5.17a_0)$ (red circle) and $(x_4, y_4) = (-2.12, -6.67)$ (blue circle), respectively.

The trajectories of the vortices and antivortices at a time interval of $\Delta t = 40$ are shown in figure 2(b) by the red lines and blue lines, respectively. It is found that the vortices from the two initial VDs (1, 2 and 3, 4) recombine into new VDs (2, 3 and 1, 4) which scatter in the opposite directions. This can be understood as follows. The motion of a vortex depends
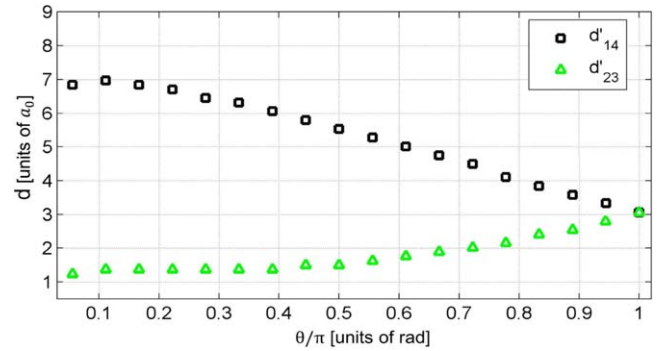
on the flow pattern of its nearby vortices [70]. This means that the vortices are usually aware of each other [71]. When the two VDs reach their minimum distance, the antivortex 2 is closer to the vortex 3 than the antivortex 4, thus the effect of the antivortex 2 on the vortex 3 plays a major role. As a result, while the antivortex 2 and the vortex 3 constitute a new VD which propagating in the $-x$ direction, the vortex 1 and the antivortex 4 form another new VD which propagating in the $+x$ direction. In figures 2(c) and 2(d), we also plot the corresponding phase distributions with the singular points picking the positions of the vortices and antivortices.

The relation between the sizes of the VDs and the collision angle θ is shown in figure 3. With the angle θ decreasing from π to $\pi/18$, while the size d'_{23} of the VD (2, 3) gets smaller, the size d'_{14} of the VD (1, 4) gets larger. This can be understood by noting that the total momentum before the oblique collision is in the $+x$ direction, and the system with smaller angle θ has larger total momentum. It is also known that a bigger VD has larger momentum [53, 72]. So after the oblique collision, we have $d'_{14} > d'_{23}$, and the smaller angle θ makes bigger size of d'_{14} and smaller size of d'_{23}.

For the oblique collisions of two VDs with the same size, the size of the VD (2, 3) generated by the vortex recombination is always smaller than those of the initial VDs (1, 2 and 3, 4). A natural question is whether VD annihilation can occur when the sizes of the initial VDs is small enough. And if so, what is the critical size of the initial VDs. To answer this question, we have performed numerical simulations on the collisions of two VDs with different sizes and moving directions. Specially, when $d_{12} = d_{34} = 1.25a_0$ and $\theta = \pi/3$, from the trajectories of the vortex and antivortex in a time interval $\Delta t = 16$, as shown in figure 4(b), one finds that after the oblique collision while the vortex 1 and antivortex 4 combine into a new VD moving in the $+x$ direction, the antivortex 2 and vortex 3 annihilate and generate a dark soliton, as shown in the dashed square of figure 4(b). From the phase distributions, one can see that the phase singularities are no longer discernible [50] in the region of dark soliton. Figure 5 shows the parameter-space phase diagram of the dynamics on vortex recombination and vortex
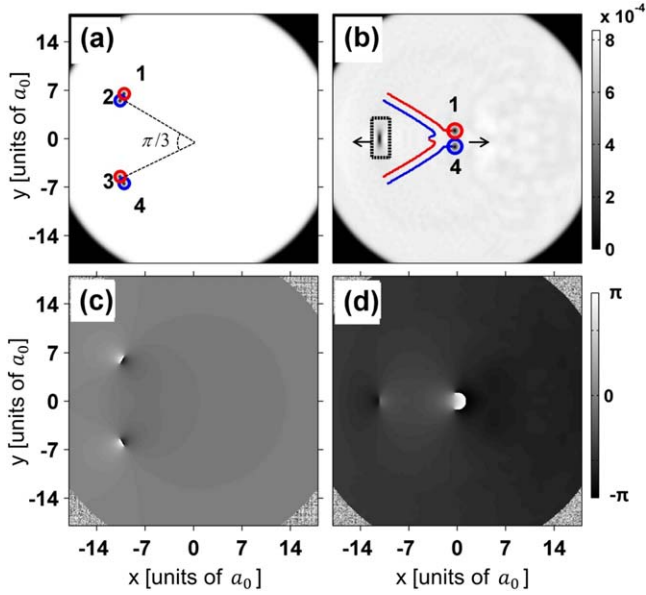
Figure 4. Vortex annihilation in the oblique collision dynamics. (a) The initial coordinates of the vortices are chosen as $(x_1, y_1) = (-10.07a_0, 6.53a_0)$ (red circle), $(x_2, y_2) = (-10.69a_0, 5.45a_0)$ (blue circle), $(x_3, y_3) = (-10.69a_0, -5.45a_0)$(red circle) and $(x_4, y_4) = (-10.07a_0, -6.53a_0)$ (blue circle). Then we have $d_{12} = d_{34} = 1.25a_0$ and $\theta = \pi/3$. (b) The trajectories of the vortices (red lines) and antivortices (blue lines) at a time interval of $\Delta t = 16\omega_c^{-1}$. The antivortex 2 and the vortex 3 annihilate and generate a dark soliton, as shown in the dashed square. The arrows indicate the propagation directions of the VD and dark soliton after collision. The corresponding phase distributions for $t = 0$ and $t = 16\omega_c^{-1}$ are shown in (c) and (d).
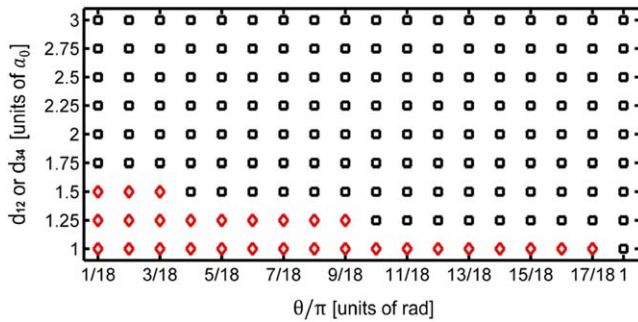

Figure 5. Parameter-space phase diagram of the oblique collision dynamics. While the black squares indicate the range of vortex recombination, the red diamonds indicate the range of vortex annihilation.

Figure 6. Catching-up dynamics of two vortex dipoles with a large vortex distance. (a$_1$) The initial coordinates of the vortices are $(x_1, y_1) = (-12a_0, 1.3a_0)$ (red circle), $(x_2, y_2) = (-12a_0, -1.3a_0)$ (blue circle), $(x_3, y_3) = (-5a_0, 2a_0)$ (red circle) and $(x_4, y_4) = (-5a_0, -2a_0)$ (blue circle). The vortex distances of the VDs are $d_{12} = 2.6a_0$ and $d_{34} = 4_0$. (b$_1$) The positions of the vortices at $t = 14.4\omega_c^{-1}$. (c$_1$) The trajectories of the vortices (red lines) and antivortices (blue lines) at a time interval of $\Delta t = 40\omega_c^{-1}$. In figures (a$_1$)–(c$_1$), the arrows indicate the propagation directions of the VDs. The corresponding phase distributions for $t = 0$, $t = 14.4\omega_c^{-1}$ and $t = 40\omega_c^{-1}$ are shown in (a$_2$), (b$_2$) and (c$_2$).

annihilation. It can be found that VD annihilation usually occurs with smaller angle θ and smaller size of the VDs.

3.2. Catching-up dynamics of two vortex dipoles

We next investigate the catching-up dynamics ($\theta = 0$) of two VDs with different sizes. Specially, we consider two VDs with the four vortices initially located on $(x_1, y_1) = (-12a_0, 1.3a_0)$ (red circle), $(x_2, y_2) = (-12a_0, -1.3a_0)$ (blue circle), $(x_3, y_3) = (-5a_0, 2a_0)$ (red circle) and $(x_4, y_4) = (-5a_0, -2a_0)$ (blue circle), as shown in
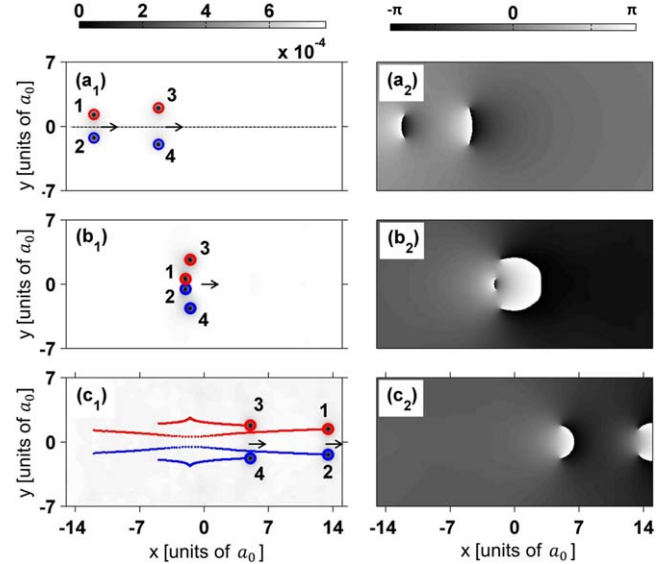
figures 6(a1)–(a2). In this case, we have $d_{12} = 2.6a_0$ and $d_{34} = 4a_0$. It is found that when the VD (1, 2) is about to pass through the VD (3,4), while the size of the VD (1, 2) becomes smaller, that of the VD (3, 4) becomes larger with $d_{12} = 1.07a_0$ and $d_{34} = 5.37a_0$, as shown in figures 6(b1)–(b2). This can be understood qualitatively as follows. When VD (1, 2) and VD (3, 4) get closer, the vortex-vortex inter-action becomes more obviously. The flow pattern of the vortex 1 is anticlockwise, which tends to drive the vortex 3 in the $+y$ direction. In contrast, the flow pattern of the antivortex 2 is clockwise, which tends to drive the antivortex 4 in the $-y$ direction. As a result, the vortex 3 and the antivortex 4 become away from each other. Besides, when the VD (1, 2) has passed through the VD (3, 4), while the flow pattern of the vortex 1 tends to drive the vortex 3 in the $-y$ direction, that of the vortex 2 tends to drive the vortex 4 in the $+y$ direction. As a result, the vortex 3 and antivortex 4 become close to each other again, as shown in figures 6(c1)–(c2). Similarly, in the catching-up process, the distance between the vortex and the antivortex in the VD (1, 2) firstly increases and then decreases. This can be obviously seen from the trajectories of the vortex and the antivortex, as shown in figure 6(c1).

By choosing a smaller size of the VD (1, 2), one can find the dynamics of vortex annihilation and vortex resurrection. Without loss of generality, we choose $d_{12} = 1.2a_0$ and
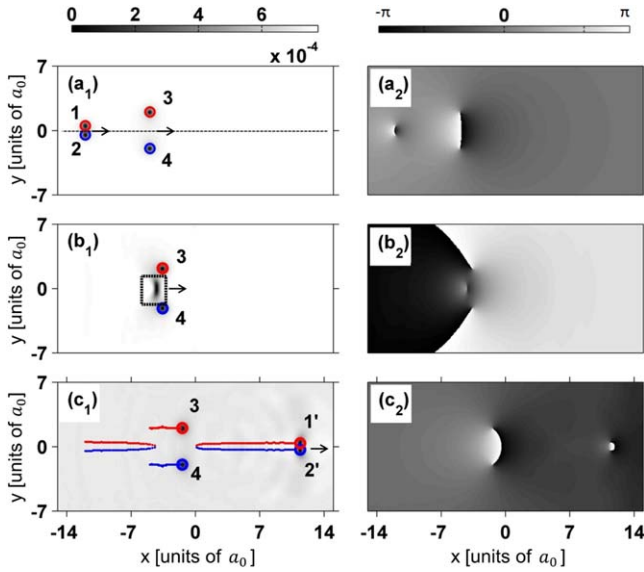
Figure 7. Vortex annihilation and vortex resurrection in the catching-up dynamics. (a_1) The initial coordinates of the vortices are $(x_1, y_1) = (-12a_0, 0.6a_0)$ (red circle), $(x_2, y_2) = (-12a_0, -0.6a_0)$ (blue circle), $(x_3, y_3) = (-5a_0, 2a_0)$ (red circle) and $(x_4, y_4) = (-5a_0, -2a_0)$ (blue circle). The initial vortex distances are $d_{12} = 1.2a_0$ and $d_{34} = 4a_0$. (b_1) The vortex 1 and the antivortex 2 temporarily annihilate at $t = 5.1$ and generate a dark soliton, as shown in the dashed square. (c_1) The trajectories of the vortices (red lines) and antivortices (blue lines) at a time interval of $\Delta t = 15\omega_c^{-1}$. The VD (1, 2) firstly annihilates and then revives again. In figures (a_1)–(c_1), the arrows indicate the propagation directions of the VDs and the dark soliton. The corresponding phase distributions for $t = 0$, $t = 5.1\omega_c^{-1}$ and $t = 15\omega_c^{-1}$ are shown in (a_2), (b_2) and (c_2).
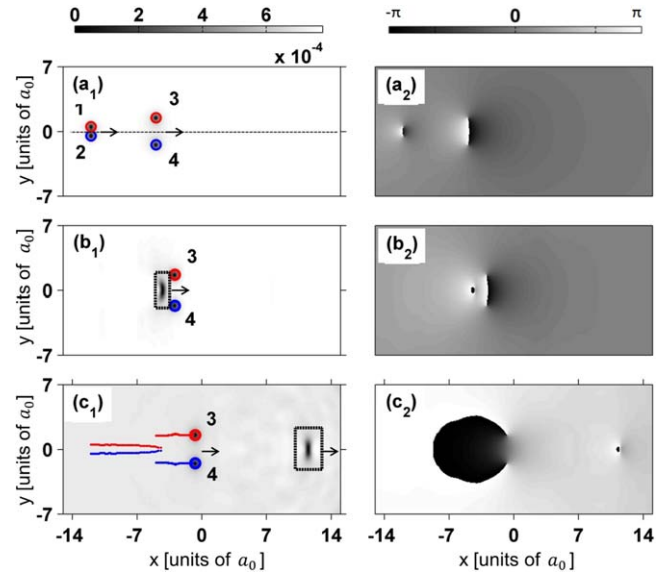
Figure 8. Vortex permanent annihilation in the catching-up dynamics. (a_1) The initial coordinates of the vortices are $(x_1, y_1) = (-12a_0, 0.6a_0)$ (red circle), $(x_2, y_2) = (-12a_0, -0.6a_0)$ (blue circle), $(x_3, y_3) = (-5a_0, 1.5a_0)$ (red circle) and $(x_4, y_4) = (-5a_0, -1.5a_0)$ (blue circle). The initial vortex distances are $d_{12} = 1.2a_0$ and $d_{34} = 3a_0$. (b_1) The vortex 1 and the antivortex 2 permanently annihilate at $t = 5.4$ and generate a dark soliton, as shown in the dashed square. (c_1) The trajectories of the vortices (red lines) and antivortices (blue lines) at a time interval of $\Delta t = 13\omega_c^{-1}$. In figures ($a_1$)-($c_1$), the arrows indicate the propagation directions of the VDs and dark soliton. The corresponding phase distributions for $t = 0$, $t = 5.4\omega_c^{-1}$ and $t = 13\omega_c^{-1}$ are shown in (a_2), (b_2) and (c_2).

$d_{34} = 4a_0$. The catching-up process is shown in figure 7. As the VD (1, 2) approaches the VD (3, 4), the vortex 1 and antivortex 2 get closer, then annihilate and generate a dark soliton, as shown in the dashed square of figures 7(b1)–(b2). Interestingly, we find that the vortices annihilation is temporary, and after passing through the VD (3, 4), the dark soliton revives the vortex dipole structure again. The vortex annihilation and resurrection can be visibly distinguished from the trajectories of the phase singularity, and when the vortices annihilate, the phase singularity will correspondingly disappear, as shown in figure 7(c1).

By further decreasing the size of the VD (3, 4), one can observe the permanent annihilation of the VD (1, 2). Figure 8 show the dynamics for the case of initial distances $d_{12} = 1.2a_0$ and $d_{34} = 3a_0$. When the VD (1, 2) approaches the VD (3, 4), vortex 1 and antivortex 2 annihilate and generate a dark soliton, as shown in figures 8(b1)–(b2). Different from the case of figure 7, the vortices annihilation is permanent, and the dark soliton does not revive the dipole structure again, as shown in figures 8(c1)–(c2).

From figures 6–8, one can find that the catching-up dynamics depends on the initial sizes of the VDs (d_{12} and d_{34}). Figure 9 shows the parameter-space phase diagram of the catching-up dynamics. While the VD (1, 2) permanently annihilates in the region with small enough d_{12} and d_{34}, the temporarily annihilated vortices can revive in the region with
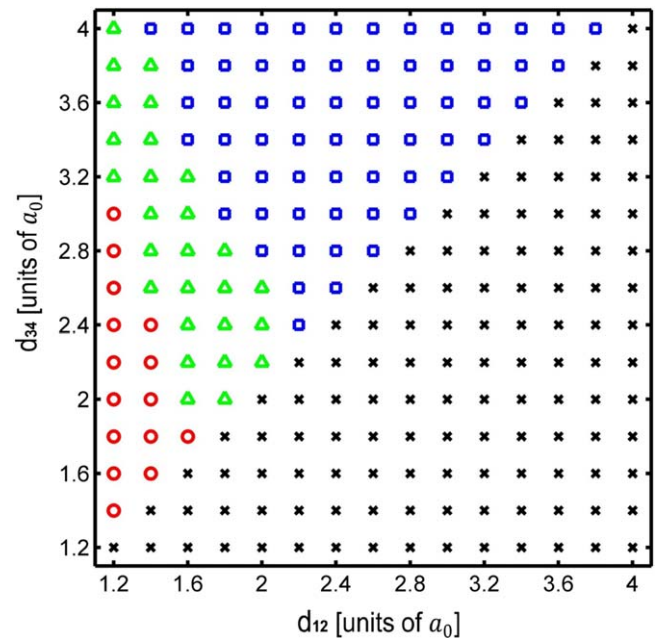

Figure 9. Parameter-space phase diagram of the catching-up dynamics. The red circles indicate that the VD (1, 2) permanently annihilates. The green triangles indicate that the VD (1, 2) temporarily annihilates and revives again. The blue squares indicate that the VD (1, 2) does not annihilate when passing through the VD(3, 4). The black crosses indicate that the VD (1, 2) can not catch up the VD(3, 4).

middle sizes of the VDs. In the region with larger enough d_{12} and d_{34}, no vortex annihilation occurs.

It has been previously indicated that the VD annihilation in a uniform system is a many-vortex process free from dissipation [50]. A VD can reduce its separation via a long-range interaction with a third catalyst vortex. By giving up some of its energy to this catalyst vortex, the vortex–antivortex can fuse and form a dark soliton [50]. In contrast, in the present system the VD annihilation results from its interaction with another VD. The VD (1, 2) reduce its separation by transferring its energy to VD (3, 4). Before the VD (1, 2) passing through the VD (3, 4), the energy of the VD (1, 2) is first transmitted to the VD (3, 4). And after passing through the VD (3, 4), the VD (3, 4) transfers energy back to the VD (1, 2). This is the reason why the VD can annihilate and revive. In addition, during the catching-up process, there exists some energy lost due to sound-wave emission [34, 55, 56]. When the size of the VD (1, 2) is small enough, after passing through the VD (3, 4), the rest energy of the VD (1, 2) is not enough to form a new vortex dipole structure again. This is the reason why the VD (1, 2) permanently annihilates. Besides, when the original size d_{12} is large enough and no vortex annihilation happens during the catching-up process, the VD (1, 2) will get smaller size and faster velocity after passing through the VD (3, 4) because of sound-wave emission.

4. The effective particle model

In this section, we would like to demonstrate that the oblique collision and catching-up dynamics can also be well described by the effective particle model [19, 45, 70, 73, 74]. When the distances of the vortices are larger than the size of the vortex core, a small cluster of n vortices can be treated as classical particles, whose kinematic equations in a uniform background take the form

$$\dot{x}_i = -b \sum_{k \neq i}^{n} S_k \frac{y_i - y_k}{r_{ik}^2}, \tag{2}$$

$$\dot{y}_i = b \sum_{k \neq i}^{n} S_k \frac{x_i - x_k}{r_{ik}^2}, \, i = 1 \ldots n, \tag{3}$$

where (x_i, y_i) are the coordinates, S_i is the charge of the ith vortex, and $r_{ik} = \sqrt{(x_i - x_k)^2 + (y_i - y_k)^2}$ denotes the separation between the vortex i and vortex k. The topological charge of the ith vortex is $S_i = \pm 1$ with the positive (negative) sign referring to counter-clockwise (clockwise) circulation as viewed from the positive z axis [70]. Here b is a positive numerical constant, and in the case of unit charge vortices, $b \approx 0.975$ was found to yield good agreement with the results obtained in the framework of GP simulation [73]. This type of modeling has been shown to be successful in describing various vortex dynamics [19, 45, 70, 73, 74]. It is convenient to rewrite the equations (2) and (3) according to our present system by setting $n = 4$ and $S_1 = -S_2 = S_3 = -S_4 = 1$. If we choose the same initial coordinates of the vortices as those of figures 2 and 6, we find that the trajectories obtained by the effective particle
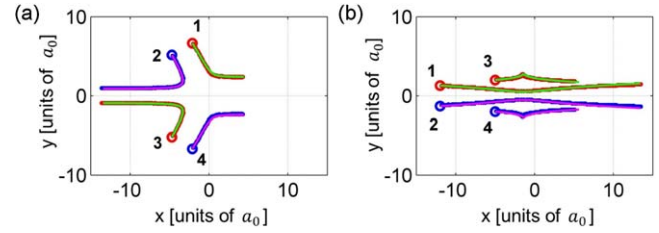

Figure 10. Comparison between the effective particle model and the Gross–Pitaevskii model on (a) the oblique collision and (b) the catching-up dynamics. The initial positions of the vortices (antivortices) are labeled by red (blue) circles. The vortex trajectories from the effective particle (Gross–Pitaevskii) modeling are depicted by green and magenta (red and blue) lines. The parameters in (a) and (b) are chosen according to figures 2 and 6, respectively.

model agree very well with those obtained by the GP simulations, as shown in figure 10.

5. Conclusions

We have investigated the oblique collision and catching-up dynamics of two vortex dipoles in a uniform Bose–Einstein condensate. We find that the collision dynamics are deeply related to the moving directions and the sizes of the initial vortex dipoles. For the oblique collisions of two vortex dipoles with the same size, we observe recombination and annihilation of the vortex dipoles. For the catching-up processes of two vortex dipoles with different sizes, we observe vortex temporary annihilation and resurrection, as well as vortex permanent annihilation. The corresponding parameter-space phase diagrams of the dynamics are given by numerical simulations. The oblique collision and catching-up dynamics of vortex dipoles discussed here usually occurs in systems of quantum turbulence. Our present study may contribute to a further understanding of the non-equilibrium physics in quantum fluids.

ORCID iDs

Suying Zhang ⓘ https://orcid.org/0000-0002-9243-7933

References

[1] Lugt H J 1995 *Vortex Flow in Nature and Technology* (Malabar, FL: Krieger Publishing Company)
[2] Freund I 2001 *Opt. Commun.* **199** 47
[3] Donnelly R J 1991 *Quantized Vortices in Hellium II[M]* (Cambridge: Cambridge University Press)

[4] Blatter G *et al* 1994 *Rev. Mod. Phys.* **66** 1125
[5] Butts D A and Rokhsar D S 1999 *Nature* **397** 327
[6] Svidzinsky A A and Fetter A L 2000 *Phys. Rev. Lett.* **84** 5919
[7] Matthews M R, Anderson B P, Haljan P C, Hall D S, Wieman C E and Cornell E A 1999 *Phys. Rev. Lett.* **83** 2498
[8] Gertjerenken B, Kevrekidis P G, Carretero-González R and Anderson B P 2016 *Phys. Rev.* A **93** 023604
[9] Engels P, Coddington I, Haljan P C and Cornell E A 2002 *Phys. Rev. Lett.* **89** 100403
[10] Coddington I, Engels P, Schweikhard V and Cornell E A 2003 *Phys. Rev. Lett.* **91** 100402
[11] Smith N L, Heathcote W H, Krueger J M and Foot C J 2004 *Phys. Rev. Lett.* **93** 080406
[12] Schweikhard V, Coddington I, Engels P, Tung S and Cornell E A 2004 *Phys. Rev. Lett.* **93** 210403
[13] Tung S, Schweikhard V and Cornell E A 2006 *Phys. Rev. Lett.* **97** 240402
[14] Dai C Q, Zhou G Q, Chen R P, Lai X J and Zheng J 2017 *Nonlinear Dyn.* **88** 2629–35
[15] Wang Y Y, Chen L, Dai C Q, Zheng J and Fan Y 2017 *Nonlinear Dyn.* **90** 1269–75
[16] Crasovan L C, Vekslerchik V, Pérez-García V M, Torres J P, Mihalache D and Torner L 2003 *Phys. Rev.* A **68** 063609
[17] Mottonen M, Virtanen S M M, Isoshima T and Salomaa M M 2005 *Phys. Rev.* A **71** 033626
[18] Pietila V, Mottonen M, Isoshima T, Huhtamaki J A M and Virtanen S M M 2006 *Phys. Rev.* A **74** 023603
[19] Torres P J, Carretero-González R, Middelkamp S, Schmelcher P, Frantzeskakis D J and Kevrekidis P G 2011 *Commun. Pure Appl. Anal.* **10** 1589
[20] Yang T, Hu Z-Q, Zou S and Liu W-M 2016 *Sci. Rep.* **6** 29066
[21] Crasovan L C, Molina-Terriza G, Torres J P, Torner L, Pérez-García V M and Mihalache D 2002 *Phys. Rev.* E **66** 036612
[22] Neely T W, Samson E C, Bradley A S, Davis M J and Anderson B P 2010 *Phys. Rev. Lett.* **104** 160401
[23] Kwon W J, Seo S W and Shin Y 2015 *Phys. Rev.* A **92** 033613
[24] Kwon W J, Kim J H, Seo S W and Shin Y 2016 *Phys. Rev. Lett.* **117** 245301
[25] Voropayev S I and Afanasyev Y D 1994 *Vortex Structures in a Stratified Fluid: Order from Chaos* (London: Chapman and Hall)
[26] Ginzburg A and Fedorov K 1984 *Dokl. Akad. Nauk SSSR* **274** 481
[27] Couder Y and Basdevant C 1986 *J. Fluid Mech.* **173** 225
[28] Roumpos G *et al* 2011 *Nat. Phys.* **7** 129
[29] Nardin G *et al* 2011 *Nat. Phys.* **7** 635
[30] Barenghi C F, Donnelly R J and Vinen W F (ed) 2001 *Quantized Vortex Dynamics and Superfluid Turbulence* vol 571 (Berlin: Springer)
[31] Kobayashi M and Tsubota M 2005 *Phys. Rev. Lett.* **94** 065302
[32] Horng T L, Hsueh C H and Gou S C 2008 *Phys. Rev.* A **77** 063625
[33] Nazarenko S and Onorato M 2007 *J. Low Temp. Phys.* **146** 31
[34] Nazarenko S and Onorato M 2006 *Physica* D **219** 1
[35] Tsubota M, Kobayashi M and Takeuchi H 2013 *Phys. Rep.* **522** 191
[36] Berezinskii V L 1972 *Sov. Phys. JETP* **34** 610 www.jetp.ac.ru/cgi-bin/e/index/e/34/3/p610?a=list
[37] Kosterlitz J M and Thouless D J 1973 *J. Phys.* C **6** 1181
[38] Hadzibabic Z *et al* 2006 *Nature* **441** 1118
[39] Zurek W H 1985 *Nature* **317** 505
[40] Anglin J R and Zurek W H 1999 *Phys. Rev. Lett.* **83** 1707
[41] Svistunov B V 1991 *J. Mosc. Phys. Soc.* **1** 373
[42] Weiler C N *et al* 2008 *Nature* **455** 948
[43] Freilich D V, Bianchi D M, Kaufman A M, Langin T K and Hall D S 2010 *Science* **329** 1182
[44] Kuopanportti P, Huhtamaäki J A M and Möttönen M 2011 *Phys. Rev.* A **83** 011603(R)
[45] Middelkamp S, Torres P J, Kevrekidis P G, Frantzeskakis D J, Carretero-González R, Schmelcher P, Freilich D V and Hall D S 2011 *Phys. Rev.* A **84** 011605(R)
[46] Prabhakar S, Singh R P, Gautam S and Angom D 2013 *J. Phys. B: At. Mol. Opt. Phys.* **46** 125302
[47] Kwon W J, Moon G, Choi J-Y, Seo S W and Shin Y-I 2014 *Phys. Rev.* A **90** 063627
[48] Stagg G W, Allen A J, Parker N G and Barenghi C F 2015 *Phys. Rev.* A **91** 013612
[49] Du Y, Niu C, Tian Y and Zhang H 2015 *J. High Energy Phys.* **12** 018
[50] Groszek A J, Simula T P, Paganin D M and Helmerson K 2016 *Phys. Rev.* A **93** 043614
[51] Feijoo D, Paredes A and Michinel H 2017 *Phys. Rev.* E **95** 032208
[52] Aioi T, Kadokura T and Saito H 2012 *Phys. Rev.* A **85** 023618
[53] Aioi T, Kadokura T, Kishimoto T and Saito H 2011 *Phys. Rev.* X **1** 021003
[54] Smirnov L A and Smirnov A I 2015 *Phys. Rev.* A **92** 013636
[55] Barenghi C F, Parker N G, Proukakis N P and Adams C S 2005 *J. Low Temp. Phys.* **138** 629
[56] Griffin A, Stagg G W, Proukakis N P and Barenghi C F 2017 *J. Phys.* B **50** 115003
[57] Yang G Q, Zhang S Y and Jin J J 2019 *J. Phys. B: At. Mol. Opt. Phys.* **52** 065201
[58] Gaunt A L, Schmidutz T F, Gotlibovych I, Smith R P and Hadzibabic Z 2013 *Phys. Rev. Lett.* **110** 200406
[59] Chomaz L, Corman L, Bienaimé T, Desbuquois R, Weitenberg C, Nascimbène S, Beugnon J and Dalibard J 2015 *Nat. Commun.* **6** 6162
[60] Manek I, Ovchinnikov Y B and Grimm R 1998 *Opt. Commun.* **147** 67
[61] Bao W, Jaksch D and Markowich P A 2003 *J. Comput. Phys.* **187** 318
[62] Yang S J, Wu Q S, Zhang S N, Feng S, Guo W, Wen Y C and Yu Y 2007 *Phys. Rev.* A **76** 063606
[63] Ding D J, Jin D Q and Dai C Q 2017 *Therm. Sci.* **21** 4
[64] White A C, Barenghi C F and Proukakis N P 2012 *Phys. Rev.* A **86** 013635
[65] Matthews M R, Anderson B P, Haljan P C, Hall D S, Wieman C E and Cornell E A 1999 *Phys. Rev. Lett.* **83** 2498
[66] Williams J E and Holland M J 1999 *Nature* **401** 568–72
[67] Andrelczyk G, Brewczyk M, Dobrek Ł, Gajda M and Lewenstein M 2001 *Phys. Rev.* A **64** 043601
[68] Bao W and Wang H Q 2006 *J. Comput. Phys.* **217** 612
[69] Caradoc-Davies B M 2000 Vortex dynamics in Bose–Einstein condensates *PhD Thesis* University of Otago, New Zealand
[70] Torres P J, Kevrekidis P G, Frantzeskakis D J, Carretero-Gonzalez R, Schmelcher P and Hall D S 2011 *Phys. Lett.* A **375** 3044
[71] Sakhel R R and Sakhel A R 2016 *J. Low Temp. Phys.* **184** 1–22
[72] Crescimanno M, Koay C G, Peterson R and Walsworth R 2000 *Phys. Rev.* A **62** 063612
[73] Middelkamp S, Kevrekidis P G, Frantzeskakis D J, Carretero-González R and Schmelcher P 2010 *Phys. Rev.* A **82** 013646
[74] Navarro R, Carretero-González R, Torres P J, Kevrekidis P G, Frantzeskakis D J, Ray M W, Altuntas E and Hall D S 2013 *Phys. Rev. Lett.* **110** 225301